Cerebral Cortex April 2014;24:1088–1101
doi:10.1093/cercor/bhs375
Advance Access publication December 16, 2012

Accumulation of GABAergic Neurons, Causing a Focal Ambient GABA Gradient, and Downregulation of *KCC2* Are Induced During Microgyrus Formation in a Mouse Model of Polymicrogyria

Tianying Wang[1], Tatsuro Kumada[1], Toshitaka Morishima[1], Satomi Iwata[1], Takeshi Kaneko[2], Yuchio Yanagawa[3,4], Sachiko Yoshida[5] and Atsuo Fukuda[1]

[1]Department of Neurophysiology, Hamamatsu University School of Medicine, Hamamatsu, Shizuoka 431-3192, Japan [2]Department of Morphological Brain Science, Graduate School of Medicine, Kyoto University, Kyoto 606-8501, Japan [3]Department of Genetic and Behavioral Neuroscience, Gunma University Graduate School of Medicine, Maebashi, Gunma 371-8511, Japan [4]Japan Science and Technology Agency, CREST, Tokyo 102-0075, Japan and [5]Department of Environmental and Life Sciences, Toyohashi University of Technology, Toyohashi, Aichi 441-8580, Japan

Address correspondence to Atsuo Fukuda, Department of Neurophysiology, Hamamatsu University School of Medicine, 1-20-1 Handayama, Hamamatsu, Shizuoka 431-3192, Japan. Email: axfukuda@hama-med.ac.jp

Although focal cortical malformations are considered neuronal migration disorders, their formation mechanisms remain unknown. We addressed how the γ-aminobutyric acid (GABA)ergic system affects the GABAergic and glutamatergic neuronal migration underlying such malformations. A focal freeze-lesion (FFL) of the postnatal day zero (P0) glutamic acid decarboxylase–green fluorescent protein knock-in mouse neocortex produced a 3- or 4-layered microgyrus at P7. GABAergic interneurons accumulated around the necrosis including the superficial region during microgyrus formation at P4, whereas E17.5-born, Cux1-positive pyramidal neurons outlined the GABAergic neurons and were absent from the superficial layer, forming cell-dense areas in layer 2 of the P7 microgyrus. GABA imaging showed that an extracellular GABA level temporally increased in the GABAergic neuron-positive area, including the necrotic center, at P4. The expression of the Cl^- transporter *KCC2* was downregulated in the microgyrus-forming GABAergic and E17.5-born glutamatergic neurons at P4; these cells may need a high intracellular Cl^- concentration to induce depolarizing GABA effects. Bicuculline decreased the frequency of spontaneous Ca^{2+} oscillations in these microgyrus-forming cells. Thus, neonatal FFL causes specific neuronal accumulation, preceded by an increase in ambient GABA during microgyrus formation. This GABA increase induces $GABA_A$ receptor-mediated Ca^{2+} oscillation in *KCC2*-downregulated microgyrus-forming cells, as seen in migrating cells during early neocortical development.

Keywords: γ-aminobutyric acid, focal freeze-lesion, KCC2, microgyrus, neuronal migration

Introduction

Neocortical malformations, such as polymicrogyria, show the presence of cortical cells in heterotopic positions; this is often caused by disruption in neuronal migration (for reviews, see Walsh 1999; Francis et al. 2006). The focal freeze-lesion (FFL) induces microgyrus, a focal cortical malformation with a small sulcus, and a 3- or 4-layered microgyric cortex, which resembles human 4-layered microgyria (Dvorák and Feit 1977; Dvorák et al. 1978). Electrophysiological studies have revealed that epileptiform activity can be initiated within a few millimeters of a lesion-induced microgyrus (Jacobs et al. 1996; Luhmann and Raabe 1996), so the rat FFL model is often used to study the mechanisms of epileptogenesis in cortical malformations (Zilles et al. 1998; Redecker et al. 2000; Hagemann et al. 2003; Jacobs and Prince 2005; Chu et al. 2009). Although this model shows an abnormal distribution of a particular population of cortical neurons in the microgyric cortex (Jacobs et al. 1996; Rosen et al. 1998; Kharazia et al. 2003; Patrick et al. 2006) and is hypothesized to result from abnormal neuronal migration (Zilles et al. 1998), it remains unclear how the distinct types of cortical neurons, particularly γ-aminobutyric acid (GABA)ergic neurons, migrate and accumulate during the formation of the microgyrus.

In the normal developing cortex, glutamatergic projection neurons and GABAergic interneurons, which have distinct origins, migrate into the cortical region along the different routes (Rakic 1972, 1988; Anderson et al. 1997, 2001; Tamamaki et al. 1997; Lavdas et al. 1999; for reviews, see Marín and Rubenstein 2001; Nadarajah and Parnavelas 2002) and settle in their final position during the first postnatal week in the rodent neocortex (Ignacio et al. 1995). Although GABA is the major inhibitory neurotransmitter, it also controls the migration of both immature cortical projection neurons and interneurons via distinct GABA receptors in the developing cortex (Behar et al. 1996, 1998, 2000, 2001; López-Bendito et al. 2003; Cuzon et al. 2006; Heck et al. 2007; Bortone and Polleux 2009; Denter et al. 2010; for reviews, see Luján et al. 2005; Heng et al. 2007; Manent and Represa 2007; Wang and Kriegstein, 2009). The early developmental roles of GABA in regulating neuronal migration depend on the GABA-mediated membrane depolarization that results from the relatively high intracellular Cl^- concentration ($[Cl^-]_i$) in immature cells (for review, see Ben-Ari 2002; Owens and Kriegstein 2002; Represa and Ben-Ari 2005; Wang and Kriegstein 2009). The high $[Cl^-]_i$ in immature neurons is generated by early expression of NKCC1 and delayed expression of KCC2; the latter is a key molecule for switching the effect of GABA from excitation to inhibition (Rivera et al. 1999; Yamada et al. 2004; for review, see Blaesse et al. 2009). A recent study has shown that GABA is involved in termination of tangential migration by modulating Ca^{2+} oscillation in migrating interneurons with the upregulation of KCC2 (Bortone and Polleux 2009; Miyoshi and Fishell 2011). Thus, the depolarizing action of GABA is essential for the migration of projection neurons and interneurons.

In addition to the rat model (Shimizu-Okabe et al. 2007), here, we have established an FFL in glutamic acid decarboxylase67–green fluorescent protein (GAD67-GFP) knock-in (KI) mice maternally injected with 5-bromo-2′-deoxyuridine (BrdU) to distinguish GABAergic and glutamatergic neurons, with identified birthdates, responsible for the formation of the FFL-induced microgyrus. We also examined the spatial pattern of extracellular GABA (Morishima et al. 2010) and the $GABA_A$ receptor sensitivity of spontaneous intracellular Ca^{2+} transients to elucidate the role of ambient GABA in microgyrus formation. Our results show that GABAergic and glutamatergic neurons differentially migrate toward the FFL, while sensing ambient GABA to modulate their intracellular Ca^{2+} transients during the formation of the microgyrus.

Materials and Methods

GAD67-GFP KI Mice

The GAD67-GFP (Δneo) transgenic mouse, referred to hereafter as the GAD67-GFP KI mouse, expresses enhanced GFP under regulation of the endogenous *GAD1* promoter (Tamamaki et al. 2003). Because GAD67 is a key enzyme for the biosynthesis of GABA and is specifically expressed in GABAergic cells, the GAD67-GFP KI mouse allowed us to analyze GABAergic cells (Tanaka et al. 2006). In our study, C57BL/6 wild-type female mice and GAD67-GFP KI male mice were mated, and the heterozygous pups were used in our experiments. Experienced wild-type mothers were selected for easy acceptance of the lesioned pups. The day of the detection of pregnancy was designated as embryonic day 0.5 (E0.5). The heterozygous pups were selected using a binocular microscope (Biological Laboratory Equipment, Maintenance and Service Ltd., Budapest, Hungary) equipped with appropriate lamps and filters. All procedures were performed in accordance with the guidelines issued by Hamamatsu University School of Medicine on the ethical use of animals for experimentation, and all efforts were made to minimize the number of animals used and their suffering.

Focal Freeze-Lesions

FFLs were made on GAD67-GFP KI pups at postnatal day 0 (P0), as previously described for the rat FFL model, but with some modifications (Shimizu-Okabe et al. 2007). Briefly, after anesthesia by hypothermia and cutting the skin overlying the cerebral cortex, a liquid nitrogen-cooled copper rod with a tip diameter of 0.5 mm was placed on the surface of the exposed calvarium for 5 s. To produce a longitudinal FFL, 3 identical freeze-lesions were made in a line near the midline in a rostrocaudal direction, with a distance of 0.5 mm between the lesions. These lesions resulted in a 2- to 3-mm-long microgyrus in the rostrocaudal direction at P7. The FFL was also made at P2 ($n = 4$) to compare the results with those at P0.

Immunohistochemistry

FFL mice (P2–P9) were anesthetized with halothane and perfused transcardially with cold saline, followed by a freshly prepared solution of 4% paraformaldehyde (PFA) in 0.1 M phosphate buffer (PB), pH 7.4. The brains were rapidly removed and post fixed for 3 h in 4% PFA/0.1 M PB at 4 °C. Twenty-five-micrometer thick coronal sections were cut with a cryostat (HM400R; Zeiss Microm, Walldorf, Germany) and collected in cold 0.1 M PB. Coronal sections at the level of the lesioned region were selected for immunofluorescent staining and imaging analysis. Sections were mounted on gelatin-coated slides and stained with thionin for morphological identification. For immunohistochemistry, sections were blocked for 1 h in 10% normal goat serum in 0.1 M PB with 0.2% Triton X-100 at room temperature (RT) and then incubated with primary antibodies overnight at 4 °C. The following primary antibodies were used: BrdU (1:400; Becton Dickinson, San Jose, CA, USA), GFP (rabbit, 1:1000; Molecular Probes, Eugene, OR, USA; chicken, 1:500; Aves Labs, Tigard, OR, USA), Cux1 (1:200; Santa Cruz Biotechnology, Inc., Santa Cruz, CA, USA), Tbr1 (1:500; Abcam, Billerica, MA, USA), Ki67 (1:100; Biocare Medical, Concord, CA, USA), glial fibrillary acidic protein (GFAP; 1:10 000; Dako, Glostrup, Denmark), and Iba1 (1:1000; Wako, Osaka, Japan). The sections were then washed with 0.1 M PB and incubated with secondary antibodies diluted in blocking buffer: Alexa Fluor 488 anti-rabbit IgG, Alexa Fluor 594 anti-mouse IgG (1:1000; Molecular Probes), or Cy2 anti-chicken IgY (1:100; Jackson ImmunoResearch Laboratories, West Grove, PA, USA) for 1 h at RT. Sections were washed with 0.1 M PB, mounted on slides, and observed using a fluorescence microscope (AX80T; Olympus, Tokyo, Japan) equipped with a digital camera (DP70; Olympus) or a 2-photon excitation microscope (LSM7MP; Zeiss, Jena, Germany) with a Chameleon Vision II laser system (Coherent, Inc., Santa Clara, CA, USA). For 2-photon imaging of GFP and Alexa Fluor, wavelengths of 900 and 800 nm were used and their fluorescence emissions were collected with 500- to 550-nm and 565- to 610-nm filter settings, respectively.

BrdU Labeling

Pregnant mice were intraperitoneally (i.p.) injected on either E14.5 or E17.5 with a single dose of the S-phase marker BrdU (50 mg/kg body weight; Sigma-Aldrich, St. Louis, MO, USA), which was dissolved in sterile saline (5 mg/mL) and filtered (0.22 μm). Brain sections of pups were incubated for 1 h in 2 M HCl at 37 °C before being subjected to immunohistochemistry for BrdU.

Cell Counting

For P7 freeze-lesioned sections, 2 microgyric cell-count square frames (100 μm × 100 μm) were placed both medial and lateral to a pseudosulcus through the layer 2 of the microgyrus. As controls for E17.5 BrdU-positive cells, 2 identical frames were placed 500 μm from the microgyrus both medial and lateral of the superficial layer and 50 μm from the pia. As controls for E14.5 BrdU-positive cells, 2 cell-count frames were placed underneath those for the E17.5 BrdU-positive cells, with 50 μm between the frames. All the control frames were used as controls for GFP-positive cells. Cell densities were expressed as the average number of E14.5 BrdU-, E17.5 BrdU-, or GFP-positive cells per frame. Cells overlapping the borders of the frames were not included in the cell count.

For immunofluorescence of P4 freeze-lesioned sections, one cell-count square frame (50 μm × 50 μm) was set in the superficial layer of the lesioned cortex, and 2 cell-count frames were set in both the inner and outer rim, as well as in both medial and lateral of the surrounding layer, respectively, within 100 μm of the lesion border. Exofocal frames were placed both medial and lateral of the superficial layer, >200 μm from the lesion border and 50–100 μm from the pia. For quantification of BrdU/Cux1 and BrdU/Tbr1 double-positive cells, 3 cell-count square frames (50 μm × 50 μm) were randomly placed in the surrounding (medial, deeper, and lateral) layers within 100 μm of the lesion border. For both P4 and P7 preparations, the cell-count square frames were used as the samples and the numbers of cells within them were used for statistical analyses.

In Situ Hybridization

Total RNA was prepared from the mouse cerebral cortex with Isogene reagent (Nippon Gene, Tokyo, Japan). RNA (1 μg) was used for first-strand cDNA synthesis with SuperScript II RT (Invitrogen, Carlsbad, CA, USA) with random hexamers according to the manufacturer's instructions. Polymerase chain reaction (PCR) was performed using HotStarTaq (Qiagen, Hilden, Germany). The primer sequences were as follows (all 5′–3′): *KCC2*: forward, gatgaagaaggacctgacca; reverse, gccgtacattggactggttc; *CXCL12*: forward, ctgtagcctgacggaccaat; reverse, gtggcttcatggcaagattc; and *CXCR4*: forward, tcgagagcatcgtgcacaag; reverse, cacaggtcctgcctagacac. The PCR products were cloned into the pGEM-T easy vector (Promega, Madison, WI, USA) according to the manufacturer's instructions. The orientation of the insert was confirmed by restriction mapping. After linearization with the restriction enzymes NcoI and SalI, digoxigenin (DIG)-labeled antisense and sense cRNA probes were prepared by in vitro transcription using the DIG RNA Labeling Mix (Roche Diagnostics GmbH, Mannheim,

Germany). For in situ hybridization, coronal brain sections of 16-μm thickness were prepared from FFL mice at different stages. All subsequent steps were performed at RT unless noted. Sections were fixed for 10 min in 4% PFA/0.1 M PB, washed, and treated for 15–20 min with proteinase K (10 μg/mL; Roche Diagnostics GmbH) at 37 °C. Tissue sections were fixed again in 4% PFA/0.1 M PB and treated with 0.25% acetic anhydride in 0.1 M triethanolamine for 10 min. After dehydration with ethanol, sections were incubated in hybridization buffer (50% formamide, 10% dextran sulfate, 1× Denhardt's reagent, 10 mM Tris–HCl [pH 8.0], 0.3 M NaCl, 1 mM ethylenediaminetetraacetic acid, 0.5% sodium dodecyl sulfate, and 500 μg/mL yeast tRNA) for 1 h and hybridized overnight at 56 °C in fresh hybridization buffer containing a DIG-labeled probe (1 μg/mL). Sections were subjected to sequential washes in 4×, 2×, 1×, 0.5×, and 0.05× saline-sodium citrate at 70 °C. Hybridized probe was detected using an alkaline phosphatase-conjugated anti-DIG antibody (1:1000; Roche Diagnostics GmbH) and visualized with nitro blue tetrazolium/5-bromo-4-chloro-3-indolyl phosphate (Roche Diagnostics GmbH).

Double Labeling With In Situ Hybridization and Immunohistochemistry

Following in situ hybridization histochemistry, sections were further processed to detect GFP or BrdU immunoreactivity. Sections were incubated with anti-heat-denatured GFP rabbit antibody (1 μg/mL; Nakamura et al. 2008) overnight at RT, or anti-BrdU antibody (1:400) overnight at 4 °C. Sections were further incubated with biotinylated anti-rabbit (1:100; Vector Laboratories, Burlingame, CA, USA) or anti-mouse IgG antibodies (1:100; Vector Laboratories) for 3 h at RT. After incubation at RT for 3 h with an avidin–biotinylated peroxidase complex (ABC-Elite Kit; Vector Laboratories), diluted 1:50 with 0.05 M phosphate-buffered saline (pH 7.4) containing 0.3% (v/v) Triton X-100, the bound peroxidase was developed by reaction with 0.02% (w/v) diaminobenzidine·4HCl and 0.01% (v/v) H_2O_2 in 50 mM Tris–HCl (pH 7.6).

Brain Slice Preparation

Cortical slices were prepared from P2, P4, and P7 freeze-lesioned GAD67-GFP KI pups. Animals were deeply anesthetized with halothane and then decapitated. The brains were quickly removed and placed into ice-cold oxygenated, modified artificial cerebrospinal fluid (ACSF; in mM, 220 sucrose, 2.5 KCl, 1.25 NaH_2PO_4, 12.0 $MgSO_4$, 0.5 $CaCl_2$, 26.0 $NaHCO_3$, 30.0 glucose at pH 7.4). Coronal slices (350 μm) of the neocortex were cut in the modified ACSF using a vibratome (VT-1000S; Leica, Bensheim, Germany). Only coronal slices at the level of the FFL were included in the study. Slices were allowed to recover for 90 min on nylon meshes (with 1-mm pores) placed on dishes and submerged in standard ACSF consisting of (in mM): 126 NaCl, 2.5 KCl, 1.25 NaH_2PO_4, 2.0 $MgSO_4$, 2.0 $CaCl_2$, 26.0 $NaHCO_3$, and 20.0 glucose, saturated with 95% O_2/5% CO_2 at RT.

GABA and Glutamate Imaging

We have recently developed an immobilized enzyme-linked method for GABA imaging (Morishima et al. 2010). This method employs an enzyme-linked assay system using GABase, which can catabolize GABA with simultaneous production of a fluorescent reduced form of β-nicotinamide adenine dinucleotide phosphate ($NADP^+$), NADPH. The method allows us to image extracellular GABA in acute slices. To immobilize the GABase on the surface of a quartz glass (Kanayama Rika, Nagoya, Japan), the glass was incubated in chloroform solution containing 6.6% (3-aminopropyl) triethoxysilane for 3 min before treatment with 1% glutaraldehyde in 0.5 M phosphate-buffered saline for 10 min. Then the quartz glass was incubated in 0.5 units GABase (Sigma-Aldrich)/ACSF overnight. Slices were prepared with a vibratome, then placed onto the quartz glass and perfused with ACSF containing 20 μM $NADP^+$ (Sigma-Aldrich) and α-ketoglutarate saturated with 95% O_2/5% CO_2 at RT. Such an assay can also be modified to detect extracellular glutamate (Jimbu et al. 2009). Glutamate released from the tissue can be converted to α-ketoglutarate by L-glutamate dehydrogenase (GDH), with concomitant production of a reduced form of β-NAD^+, NADH. Thus, endogenous glutamate release can be reflected by NADH fluorescence. Twenty units of GDH (Sigma-Aldrich)/ACSF were immobilized on the quartz glass. Slices were placed onto the quartz glass and perfused with ACSF containing 20 μM NAD^+ (Sigma-Aldrich) saturated with 95% O_2/5% CO_2. In the presence of GABA and/or glutamate, fluorescence was captured using an inverted fluorescence microscope (BZ-9000; Keyence, Osaka, Japan) equipped with a cooled charge-coupled device (CCD) camera. For both GABA and glutamate imaging, an ultraviolet light-emitting diode illuminating system (UV-LED; 340–350 nm; Nichia, Tokushima, Japan), in which UV light from the LED leaked onto the glass surface, was used. As NADPH or NADH fluorescence was expected to equilibrate with GABA or glutamate diffusion, respectively, an exposure time of 200 ms was used. Data were stored for offline analysis using the image-processing software (IPLab; BD Biosciences, Rockville, MD, USA). Calibration was performed after each experiment, and the calibration curve was obtained by correlating the fluorescence intensity with graded GABA or glutamate concentration (0, 10, 50, and 100 μM).

Calcium Imaging

Neurons were loaded with Rhod-3 acetoxymethyl (AM) by incubating slices using previously described procedures with some modifications (Fukuda et al. 1998; Kumada and Komuro 2004). Briefly, a dye solution of Rhod-3 AM (Invitrogen) was prepared in ACSF containing 0.01% Pluronic F-127 (Invitrogen) to a concentration of 20 μM. Coronal slices from P4 FFL mice were loaded with the dye in solution for 60 min in a tightly sealed box filled with 95% O_2/5% CO_2 at a pressure of 50 kPa at 33–35 °C, followed by incubation in standard ACSF for 30 min. Slices were then transferred to an imaging chamber on the stage of an upright microscope (BX51WI; Olympus) and continuously perfused with oxygenated ACSF at a flow rate of 2 mL/min and a temperature of 30 °C. Confocal images were obtained using a fluorescence microscope (BX51WI; Olympus) equipped with a spinning disc confocal unit (CSU-22; Yokogawa Electric, Tokyo, Japan) and an electron multiplying CCD camera (iXon DV887; Andor, Belfast, UK). A water immersion ×20 objective lens (0.5 numerical aperture; Olympus) was mounted on a piezoelectric driver (Physik Instrumente, Karlsruhe/Palmbach, Germany) with its controller (Yokogawa Electric) to allow the focal plane to be changed rapidly. Fluorophores were excited at 488 and 532 nm by a Coherent Sapphire 488–30 laser (Coherent, Inc.) and a GCL-075L laser (CrystaLaser, Reno, NV, USA) and visualized using the bandpass emission filters TXB538(2A) (Asahi Glass, Tokyo, Japan) and HQ620-60 (Chroma, Bellows Falls, VT, USA). Acquisition parameters, shutters, filter positions, and focus were controlled by IPLab software (BD Biosciences). Cells showing Rhod-3 fluorescence were randomly selected for analysis. Bicuculline methiodide (BMI; 20 μM; Sigma-Aldrich) or 6-cyano-7-nitroquinoxaline-2,3-dione (CNQX; 10 μM; Tocris, Ellisville, MO, USA) and D(–)-2-amino-5-phosphonopentanoic acid (D-AP5; 50 μM; Tocris) were bath-applied after a 20-min control recording under continuous perfusion with standard ACSF. Images were recorded after 5 min of drug application. The $[Ca^{2+}]_i$ signals were collected every 5 s with *Z*-axis increments of 5–10 μm at a depth of 40–90 μm from the first plane with detectable fluorescence. Data were stored for offline analysis using the image-processing software AquaCosmos (Hamamatsu Photonics, Hamamatsu, Japan). Only fluorescence increases at least 10% from the baseline were considered Ca^{2+} transients.

In Vivo Application of Bicuculline

Pups were i.p. injected with saline ($n = 3$) or BMI (4 mg/kg body weight, $n = 9$) every 6 h from noon of P2 until the morning of P4. Pups were perfusion-fixed with 4% PFA at 6 h (P4, $n = 9$) or 3 days (P7, $n = 3$) after the last injection. Brain sections were subjected to immunohistochemistry for GFP and Cux1 or thionin staining.

Statistical Analysis

All value ranges are given as the mean ± standard error of the mean. Statistical significance was estimated by *t*-test or 1-way analysis of variance (ANOVA) followed by post hoc testing. For the in vivo BMI application experiments, 2-way ANOVA was used. *P*-values <0.05 were considered statistically significant.

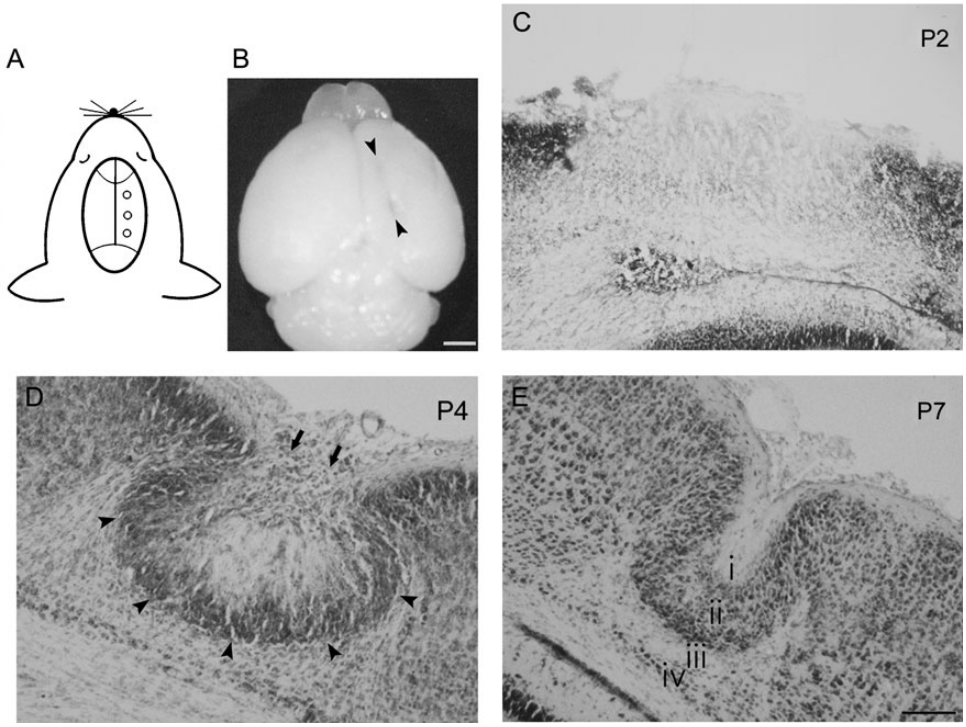

Figure 1. Morphology of freeze-lesion-induced focal cortical malformations in mice. (*A*) Schematic illustration indicating the lesioned points in the right hemisphere of a P0 GAD67-GFP KI mouse. (*B*) Dorsal view of a P7 mouse brain that received the FFL on the day of birth. A longitudinal microgyrus can be observed as an infolding of the brain surface at P7 in the right hemisphere (arrowheads). (*C–E*) Thionin-stained coronal sections at different stages. At P2, the position of the lesion was identified by necrotic tissue in the lesioned area (*C*). At P4, a cell-dense layer was observed in the superficial part (arrow) and at the boundaries (arrowheads) of the lesioned area (*D*). At P7, a microgyric architecture could be detected with a 4-layered (i, layer 1; ii, layer 2; iii, layer 3; iv, layer 4) cortex (*E*). Scale bars: *B*, 1 mm; *C–E*, 100 μm.

Results

Formation of a Microgyrus After FFL in a Mouse Model

Although many studies have shown that FFL at P0 causes cortical malformation with the microgyrus in the rat (Dvorák et al. 1978; Rosen et al. 1992; Jacobs et al. 1996; Luhmann et al. 1998; Zilles et al. 1998; Shimizu-Okabe et al. 2007), there are no reports of a similar mouse model. Because there is a species difference between the rat and mouse as regards neuronal proliferation, migration, and formation of heterotopias (DeFelipe et al. 2002; Ramos et al. 2006), we first confirmed whether FFL can form a microgyrus in heterozygous GAD67-GFP KI mice. By FFL using a rod of smaller diameter (0.5 mm) than that used in the rat, we consistently obtained typical cortical malformations consisting of a longitudinal microgyrus in the rostrocaudal direction with a length of 2–4 mm (Fig. 1*A*,*B*) by P7 ($n = 8$). We further examined the morphological development of the microgyrus after FFL at different ages from P2 to P7. The FFL initially caused focal destruction of the cortical layers on the day of birth. At P2 ($n = 2$), the position of the lesion was identified by necrotic tissue negative for thionin staining (Fig. 1*C*). At P4 ($n = 7$), a cell-dense layer was observed in the superficial region of the neocortex (arrows in Fig. 1*D*) above the necrotic tissue, which corresponds to the "bridge structure" in the rat FFL model, as described in our previous report (Shimizu-Okabe et al. 2007). We also detected a cell-dense band at the boundary (arrowheads in Fig. 1*D*) between the exofocal cortex and the lesion center. At P7, thionin staining revealed an obvious 3- or 4-layered microgyric cortex that comprised a superficial cell-sparse layer 1, a cell-dense layer 2, a deep cell-sparse layer 3, and sometimes a surviving cell layer 4 (Fig. 1*E*). These structures resembled the typical microgyrus observed in the rat model, being consistent with the evidence that the damaged cortex begins to assume its adult-like microgyric appearance from P5 to P10 in the rat FFL model (Rosen et al. 1992). Sham-operated animals ($n = 8$) did not display any abnormality in cortical structure or lamination (data not shown). Similar to the rat model (Rosen et al. 1992; Jacobs et al. 1996; Luhmann et al. 1998; Zilles et al. 1998; Shimizu-Okabe et al. 2007), cortical malformation induced by FFL in GAD67-GFP KI mice also mimicked the histological characteristics of a human 4-layered microgyrus.

E17.5-Born Glutamatergic Pyramidal Neurons Form the Cell-Dense Portions in Layer 2 of the Microgyrus

Birth-dating analysis of neurons in the microgyrus of the rat FFL model showed that late-generated neurons (from E17 to the end of neocortical neurogenesis) form the cell-dense portion of the induced microgyrus (Rosen et al. 1996). Because GABAergic and glutamatergic neurons are generated, migrate, and settle differently in the cortical region at distinct stages, we next addressed how the microgyrus is formed by migration of these distinct types of neurons. In combination with classical birth date analysis to label early- and late-born neurons using BrdU, we determined the final distribution of GABAergic neurons and E14.5- and E17.5-born cells after the formation of the microgyrus. As shown in Figure 2*A*,*D*, few E14.5-born cells set their final destination in layer 2 of the microgyrus. In contrast, many E17.5-born cells set their final

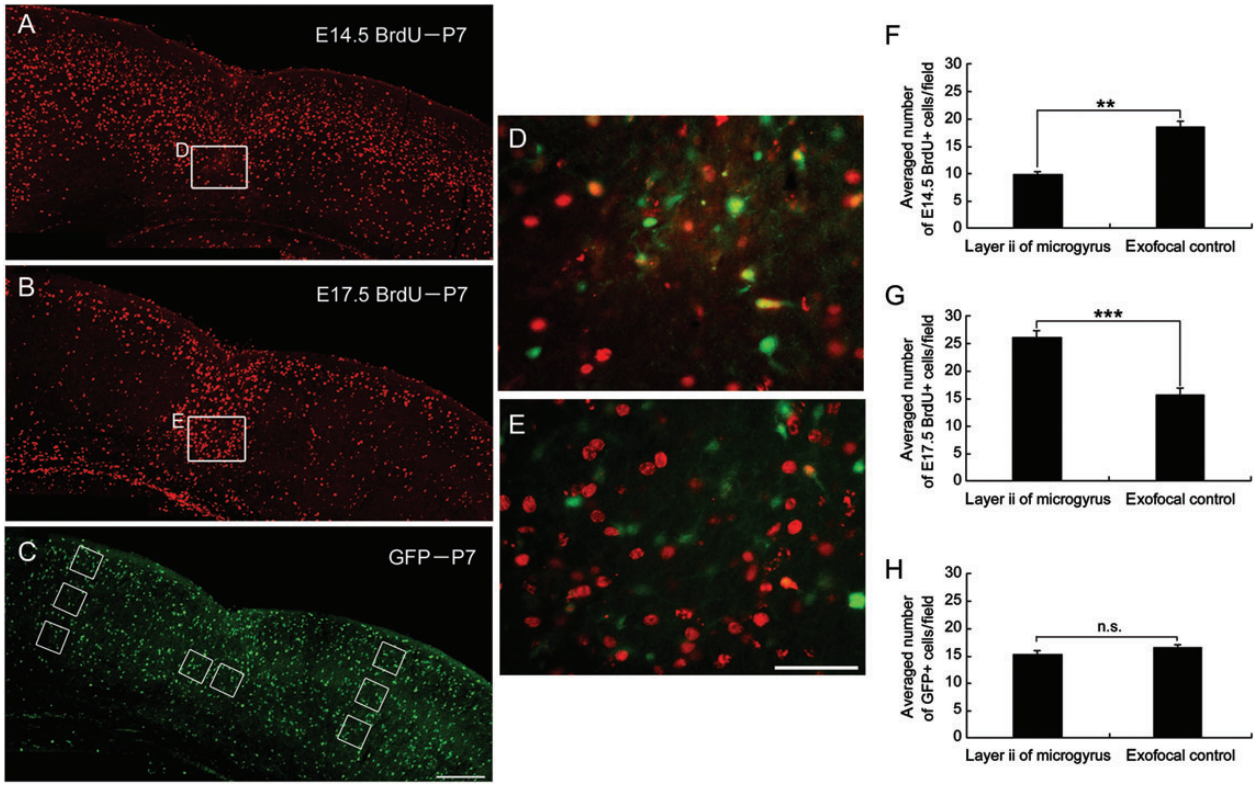

Figure 2. Distribution of E14.5- and E17.5-born cells and GABAergic cells in FFL mouse cortex at P7. Images of coronal sections of a P7 GAD67-GFP KI mouse that received a maternal injection of BrdU at E14.5 (*A*) or E17.5 (*B*), immunostained for BrdU (red). (*C*) The same P7 coronal slice as in (*B*), immunostained for GFP (green). Cell-count squares (100 μm × 100 μm) for microgyric (center) and exofocal controls (E17.5 BrdU, upper; E14.5 BrdU, middle and bottom; GFP, upper to bottom) are indicated as boxes. (*D*) Higher magnification of the boxed area in (*A*) in layer 2 of the microgyrus. There was a paucity of BrdU-positive cells (red) generated at E14.5. (*E*) Higher magnification of the boxed area in (*B*) in layer 2 of the microgyrus. Note the high density of E17.5-born, BrdU-positive cells (red) dispersed throughout layer 2 of the microgyric cortex. GFP immunostaining is also shown in *D* and *E* (green). (*F–H*) Distribution of E14.5-born BrdU-positive (3 preparations, *F*), E17.5-born BrdU-positive (4 preparations, *G*), and GFP-positive (8 preparations, *H*) cells in layer 2 of the microgyrus and the exofocal control cortex (2-tailed *t*-test, $^{**}P < 0.01$, $^{***}P < 0.001$, n.s., not significant). Scale bars: *A–C*, 200 μm; *D* and *E*, 50 μm.

destination there (Fig. 2*B*,*E*). GABAergic cells were distributed diffusely in the microgyric cortex as in the exofocal cortex (Fig. 2*C*). The number of E14.5-born, BrdU-positive cells in layer 2 of the microgyrus was significantly reduced compared with that in exofocal controls ($P < 0.001$; Fig. 2*F*), while the number of E17.5-born, BrdU-positive cells was significantly increased in layer 2 of the microgyrus ($P < 0.001$; Fig. 2*G*). These findings are consistent with a previous report that late-generated cells destined to form the upper layer invade into the necrotic center and then take their place in the unlaminated layer 2 of the rat microgyrus (Rosen et al. 1996). There was no significant difference in the number of GFP-positive GABAergic neurons in layer 2 of the microgyrus compared with that in exofocal controls ($P = 0.113$; Fig. 2*H*).

Distinct Accumulation of GABAergic and Late-Born Glutamatergic Neurons at Early Stages of the Developing Microgyrus

We next assessed the distribution pattern of the GABAergic and glutamatergic neurons during the development of the microgyrus at P4. E14.5- and E17.5-born, BrdU-positive cells were located in layers II–IV and in the superficial layer II in the exofocal cortex, respectively (Fig. 3*A* and Supplementary Fig. S1*A*), which is consistent with a previous study (Takahashi et al. 1995). GFP-positive GABAergic neurons were dispersed throughout the 6-layered exofocal cortex (Fig. 3*B* and Supplementary Fig. S1*B*). A merged BrdU and GFP image is shown in Figure 3*C*. In the lesioned cortex, few E14.5-born, BrdU-positive cells reached a final position in the area surrounding the necrotic center (Supplementary Fig. S1). In contrast, many E17.5-born, BrdU-positive neurons accumulated in the area surrounding the necrotic center (Fig. 3*A*,*E*). Interestingly, GFP-positive GABAergic cells accumulated around the lesioned area, including in the superficial area (Fig. 3*B–E*; Supplementary Fig. S1*B–E*). Quantitative analysis of the distribution of GFP-positive cells revealed that they also tended to occupy the inner rim within 50 μm of the FFL border rather than the outer rim 50–100 μm from the FFL border ($P < 0.05$; Fig. 3*F*,*G*). In contrast to GFP-positive cells, E17.5-born, BrdU-positive cells were almost absent in the superficial region of the lesioned cortex (Fig. 3*A*,*D*; $P < 0.001$; Fig. 3*H*). In addition, in contrast to GFP-positive cells, E17.5-born, BrdU-positive cells tended to occupy the outer rim rather than the inner rim ($P < 0.05$; Fig. 3*I*). GFP-positive cells were also observed within the lesioned area (Fig. 3; Supplementary Fig. S1).

In FFL mice, the distributions of GABAergic neurons and E14.5-born cells in the exofocal cortex at P4 were similar to those at P0 (Supplementary Fig. S2*A*). In contrast, E17.5-born cells whose final destination was layer II of the neocortex at P4 (Fig. 3*A*) were still in the deeper layer at P0 (Supplementary Fig. S2*B*). Thus, they had not completed radial migration when the FFL was generated.

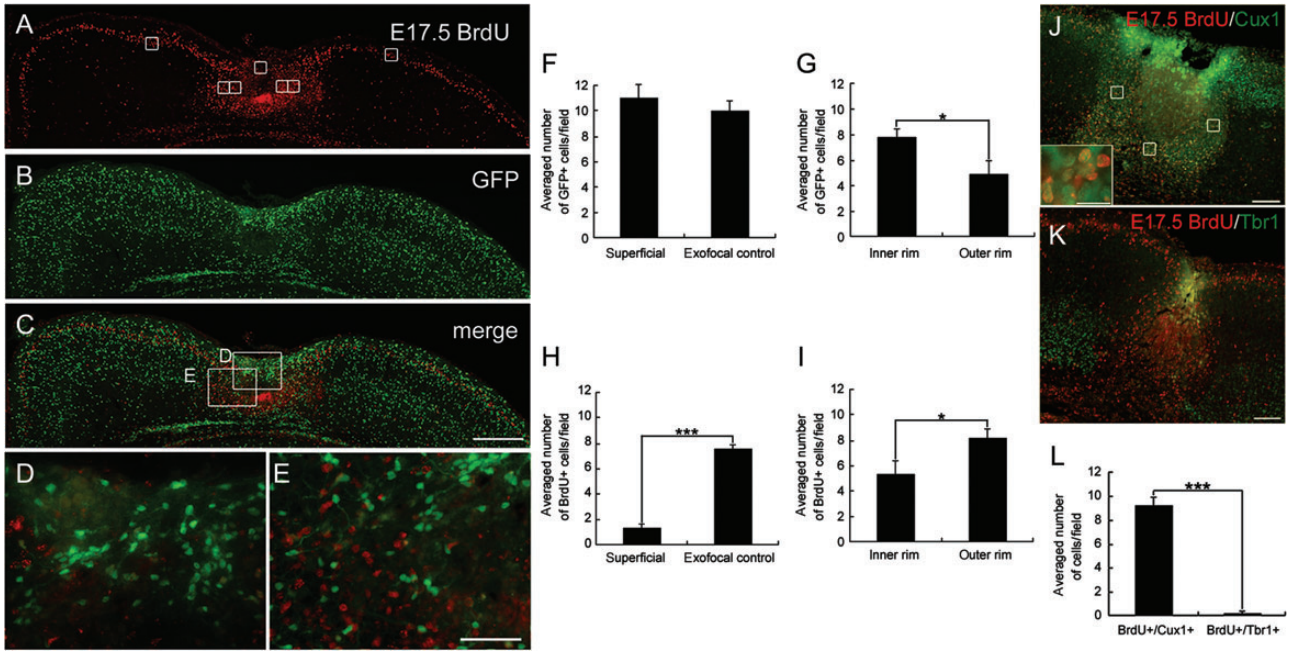

Figure 3. Distribution of E17.5-born cells and GABAergic cells in the FFL cortex at P4. Images of coronal sections of a P4 FFL mouse that received a maternal injection of BrdU at E17.5, immunostained for BrdU (red, *A*) and GFP (green, *B*). An accumulation of GFP-positive cells can be detected in the superficial part of the lesioned area (*B*). (*C*) Merged images of *A* and *B* show an accumulation of E17.5-born, BrdU-positive cells surrounding the GFP-positive cells at the boundary of the lesioned area. (*D*) Higher magnification of the superficial part of the lesion center as marked in *C*. (*E*) Higher magnification of the boundary of the lesion center as marked in (*C*). (*F* and *G*) Distribution of GFP-positive cells in the superficial region (*F*) and in the inner and the outer rim of the surrounding region within 100 μm of the lesion border (*G*). (*H* and *I*) Distribution of E17.5-born, BrdU-positive cells in the superficial region (*H*) and in the inner and the outer rim of the surrounding region (*I*). Note that there is a significant difference in the cell density of E17.5-born, BrdU-positive cells between the superficial and the exofocal regions (*H*, independent 2-tailed t-test, $^{***}P < 0.001$; 3 preparations). Note that there are significant differences in the cell densities of GFP-positive cells (*G*) and E17.5-born, BrdU-positive cells (*I*) between the inner rim and the outer rim (independent 2-tailed *t*-test, $^{*}P < 0.05$; 3 preparations each). The positions of the cell-count square frames (50 μm × 50 μm) are shown in *A*. (*J* and *K*) Images of double-staining for the layer-specific markers Cux1 (*J*) or Tbr1 (*K*) (green) and BrdU (red). A Cux1-positive cell-dense band can be observed in the area surrounding the necrotic tissue (*J*). Higher magnification shows that the majority of E17.5-born, BrdU-positive cells co-localize with Cux1 (inset in *J*). Tbr1-positive cells are absent from the microgyric cortex at P4 (*K*). (*L*) There is a significant difference in the cell density of E17.5-born, BrdU/Cux1 double-positive cells and E17.5-born, BrdU/Tbr1 double-positive cells in the surrounding region within 100 μm of the lesion border (2-tailed *t*-test, $^{***}P < 0.001$; 3 preparations each). Three cell-count square frames (50 μm × 50 μm) were placed randomly in the surrounding (medial, deeper, and lateral) layer within 100 μm of the lesion border (*J*). Scale bars: *A–C*, 200 μm; *D* and *E*, 50 μm; *J* and *K*, 100 μm; inset of *J*, 25 μm.

We further characterized the E17.5-born cells in the area surrounding the FFL using expression of layer-specific marker proteins. Cux1 is a marker specific for the pyramidal neurons of the upper layers (II–IV) of the murine cortex, and Tbr1 is a putative transcription factor, that is, highly expressed in glutamatergic early-born cortical neurons (Bulfone et al. 1995; Nieto et al. 2004). In the area surrounding the FFL, a Cux1-positive, cell-dense band was detected (Fig. 3*J*), whereas Tbr1-positive cells were absent in the area surrounding the FFL (Fig. 3*K*) at P4. In the FFL area, E17.5-born, BrdU-positive cells accumulated around the necrotic tissue and most colocalized with Cux1 (Fig. 3*J*, inset), but not with Tbr1 (Fig. 3*K*,*L*). These results suggest that the majority of E17.5-born cells that accumulated in the area surrounding the FFL were Cux1-positive glutamatergic cortical plate cells. Taken together with Figure 2, our findings in mice provide novel evidence that the supragranular neurons migrate to the damaged area within the first week after FFL, as previously suggested in the rat model (Rosen et al. 1992, 1996; Zilles et al. 1998).

Endogenous GABA Release in the Microgyrus Increases at P4

Previous studies have suggested that GABA released from GABAergic neurons has a paracrine action on immature neurons (Demarque et al. 2002; Manent et al. 2005), which may affect radial (Behar et al. 1996, 1998, 2000, 2001; Heck et al. 2007; Denter et al. 2010) and tangential (López-Bendito et al. 2003; Cuzon et al. 2006; Bortone and Polleux 2009) migration during neural development. Therefore, we next examined the spatio-temporal changes in extracellular GABA levels in the FFL cortex at different stages. We used GABA imaging, which is highly specific for its substrate, allowing accurate spatial determination of extracellular GABA levels by NADPH fluorescence (Morishima et al. 2010).

To evaluate the ambient GABA gradient, the FFL neocortex was divided into 4 parts depending on the distance from the lesion site (within lesion, and <100 μm, 100–200 μm, and >200 μm from the lesion border; Fig. 4*A*). Interestingly, intense NADPH signal was observed in and around the FFL-induced necrotic center (Fig. 4*B*). These NADPH signals disappeared if GABase was omitted (Supplementary Fig. S3*A*), indicating the accumulation of GABA. The extracellular GABA concentration in the FFL center was 42.7 ± 4.6 μM, and in the area <100 μm from the FFL border was 25.8 ± 2.6 μM; both values were significantly higher than those in the more distant areas (100–200 μm: 10.6 ± 1.2 μM and >200 μm: 9.3 ± 1.3 μM; $n = 10$; Fig. 4*C*).

We also examined glutamate, using the modified method in which glutamate is catabolized by GDH, resulting in the production of fluorescent NADH. As shown in Figure 4*D*, at P4, the ambient glutamate levels in the areas nearer to the FFL

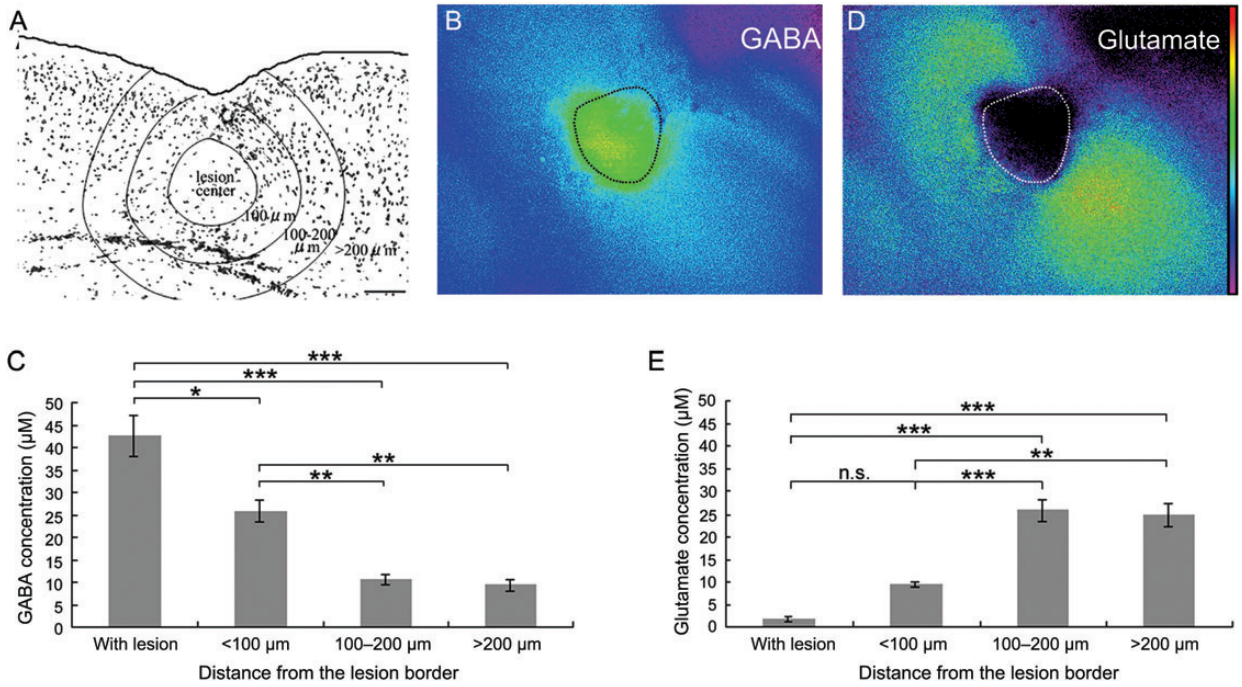

Figure 4. Temporal increase in ambient GABA in FFL. (*A*) A representative image showing the distribution of GABAergic neurons in and around the microgyric cortex at P4. (*B*) An image of extracellular GABA in a P4 acute coronal slice using an enzyme-linked assay system. The dotted line indicates the border of the necrotic tissue. (*C*) GABA concentration in the microgyric cortex at P4. The GABA concentrations in the lesion center and in the area within 100 μm of the lesion border were significantly higher than that in the area >100 μm from the lesion border (post hoc Tukey test; $*P < 0.05$, $**P < 0.01$, $***P < 0.001$, $n = 10$ slices from 6 animals). As a sample for ANOVA, fluorescence intensity was measured and averaged for each zone as indicated in *A*, from 9 randomly placed square frames (50 μm × 50 μm). (*D*) Image of extracellular glutamate in the same slice as shown in *B*. (*E*) Statistical analysis of glutamate concentration as measured similarly to GABA. The glutamate concentrations in the lesion center and in the area within 100 μm of the lesion site were significantly lower than that in the area >100 μm from the lesion site (post hoc Tukey test; $**P < 0.01$, $***P < 0.001$, n.s., not significant; $n = 3$ slices from 3 animals). Scale bars: 100 μm.

(within lesion: 1.6 ± 0.5 μM and <100 μm: 9.4 ± 0.6 μM) were much lower than those in the areas further from the FFL border (100–200 μm: 25.9 ± 2.3 μM and >200 μm: 24.8 ± 2.6 μM; $n = 3$; Fig. 4*E*).

We also measured the extracellular GABA concentration in the FFL neocortex at P2 and P7. At P2, necrotic tissue was clearly discernible, but GABA was absent in the FFL-induced necrotic tissue at this stage (Supplementary Fig. S3*B*). By P7, the concentration of extracellular GABA in the microgyric cortex became similar to that in the exofocal cortex (Supplementary Fig. S3*C*). Therefore, we speculated that the temporally increased extracellular GABA released from accumulated GABAergic neurons in the lesioned cortex might play a role in abnormal neuronal migration during the formation of the microgyrus.

Temporal Downregulation of KCC2 mRNA in Cells Accumulated in the Microgyrus at P4

The early trophic action of GABA is depolarizing, which is attributable to a high $[Cl^-]_i$ resulting in efflux of Cl^- by activation of $GABA_A$ receptors. Because temporal downregulation of KCC2 expression has been shown to occur in the microgyrus (Shimizu-Okabe et al. 2007), we set out to identify the cell type in which this downregulation occurs. We used in situ hybridization of *KCC2* mRNA in combination with BrdU or GFP immunohistochemistry. At P4, *KCC2* mRNA was strongly expressed in layer V of the exofocal cortex (Fig. 5*A*,*D*). Cells accumulated in the area surrounding the FFL lacked KCC2 (Fig. 5*B*), although moderate *KCC2* mRNA signal was detected in the BrdU-positive, E17.5-born, upper layer neurons in the exofocal cortex (Fig. 5*C*). The downregulation of *KCC2* mRNA was detected in GFP-positive GABAergic neurons accumulated in the superficial areas (Fig. 5*E*) and the area surrounding the FFL (Fig. 5*F*), whereas it was not observed in neurons residing in the exofocal area (Fig. 5*G*). By P7, strong *KCC2* mRNA signals were expressed throughout all the layers of the cortex (Fig. 5*H*), whereas its signals in BrdU-positive cells were equivalent in the microgyric and the exofocal cortices (Fig. 5*I*,*J*).

Intracellular Ca^{2+} Transients Mediated by $GABA_A$ Receptor Activation in Microgyrus-Forming Cells

Given the transient increase in ambient GABA concentration and the downregulation of *KCC2* mRNA in the lesioned cortex at P4, $GABA_A$ receptor-mediated depolarizing action may be responsible for the spontaneous Ca^{2+} oscillation that is important for the regulation of neuronal migration (for reviews, see Komuro and Kumada 2005; Spitzer 2008). To test this idea directly, we conducted calcium imaging using slices from FFL mice at P4. Figure 6*A*,*B* shows the typical spontaneous Ca^{2+} transients in P4 neocortical cells. The lesioned cortex at P4 was separated into <100 μm and >100 μm from the FFL border; the latter was further separated into the upper (<150 μm from the pia) and lower regions. The frequency of spontaneous Ca^{2+} transients was significantly higher in the cells <100 μm from the FFL border than in those

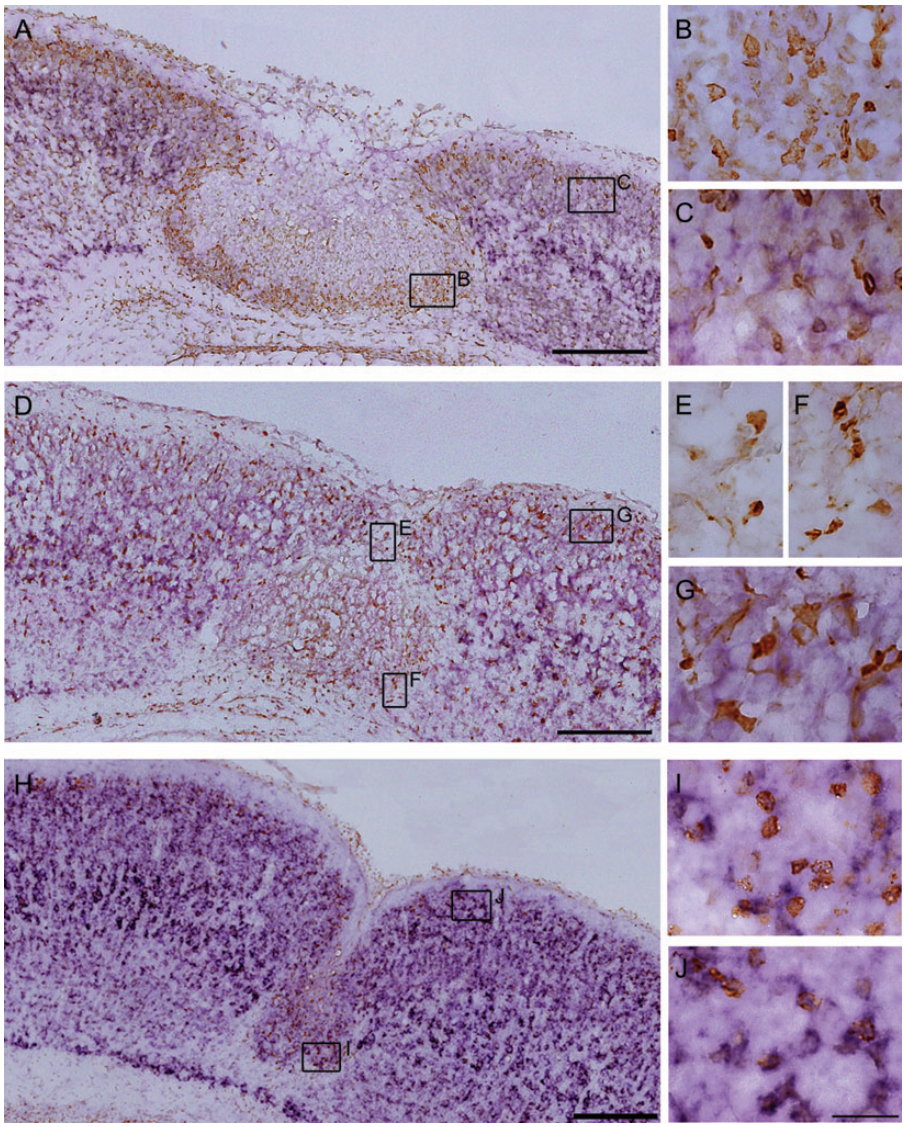

Figure 5. Counterstaining of in situ hybridization for *KCC2* mRNA with immunohistochemistry for BrdU or GFP. (*A–C*) In situ hybridization for *KCC2* mRNA (purple) combined with immunostaining for BrdU (brown) on cryosections of a P4 FFL mouse cortex that received maternal injection of BrdU at E17.5. Higher magnification of BrdU-positive neurons in the area within 100 μm of the lesion site (*B*) and in the exofocal area >100 μm from the lesion border (*C*). Note that E17.5-born, BrdU-positive neurons accumulated in the area surrounding the necrotic tissue displayed less *KCC2* mRNA expression (*B*) than those in the exofocal cortex (*C*). (*D–G*) In situ hybridization for *KCC2* mRNA (purple) combined with immunostaining for heat-denatured GFP (brown) on cryosections of a P4 FFL mouse cortex. Higher magnification of GFP-positive neurons in the superficial part of the FFL (*E*), in the area surrounding the FFL (*F*), and in the exofocal area (*G*). Note that downregulation of *KCC2* mRNA was detected in the GFP-positive GABAergic neurons in the superficial part of the FFL (*E*) and in the area surrounding the FFL (*F*), compared with that in the GABAergic neurons in the exofocal area (*G*). (*H*) In situ hybridization for *KCC2* mRNA combined with immunostaining for BrdU on cryosections of a P7 FFL mouse cortex that received maternal injection of BrdU at E17.5. *I* and *J* show higher magnification of BrdU-positive neurons in layer 2 of the microgyric cortex (*I*) and in the exofocal cortex (*J*). There was no significant difference in *KCC2* signals between the BrdU-positive neurons in the microgyric cortex (*I*) and those in the exofocal cortex (*J*). Scale bars: *A*, *D*, and *H*, 200 μm; *B*, *C*, *E*, *F*, *G*, *I*, and *J*, 25 μm.

at the further site (Fig. 6*C*; $P < 0.01$). No difference was observed between the upper and the lower parts of the exofocal area (>100 μm; Fig. 6*C*). When the $GABA_A$ receptor antagonist BMI (20 μM) was bath-applied, the number of spontaneous Ca^{2+} transients was significantly reduced only within 100 μm of the FFL border (Fig. 6*B*,*D*; $P < 0.01$). We then tested the glutamate receptor antagonists D-AP5 and CNQX, because the extracellular glutamate concentration was higher in the exofocal area (Fig. 4*D*,*E*). In contrast to BMI, the frequency of spontaneous Ca^{2+} transients was significantly reduced by D-AP5 + CNQX administration only in cells in the exofocal area (Fig. 6*E*; $P < 0.05$). These results suggest that tonic $GABA_A$ receptor-mediated depolarizing activity produces Ca^{2+} transients in migrating cells that are forming the microgyrus.

Chronic In Vivo Blockade of $GABA_A$ Receptors Perturbs the Accumulation of GABAergic and Cux1-Positive Cells and Microgyrus Formation

Next, we blocked $GABA_A$ receptors continuously in vivo after FFL to study whether the accumulation of GABAergic neurons, causing a focal ambient GABA gradient, underlies microgyrus formation. Because BMI effectively blocked the Ca^{2+} oscillation at P4 (Fig. 6), BMI was i.p. injected from P2 to P4 after FFL. At P4 ($n = 7$), the cell-dense layer in the

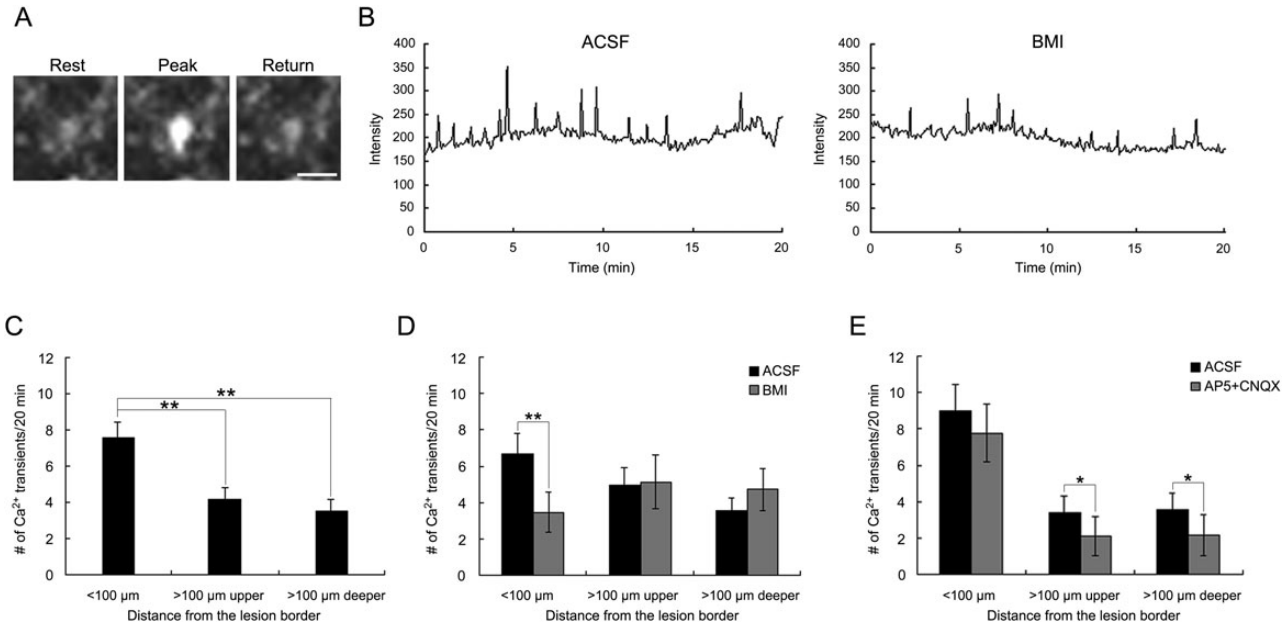

Figure 6. Spontaneous intracellular Ca^{2+} transients near the lesion site were mediated by tonic $GABA_A$ receptor activation. (*A*) Typical example of a P4 neocortical cell in the area within 100 μm of the lesion border showing spontaneous Ca^{2+} transients in its soma. (*B*) Traces of spontaneous Ca^{2+} transients before and after bath application of 20 μM BMI. (*C*) Numbers of spontaneous Ca^{2+} transients in cells in each area. The frequency of Ca^{2+} transients in the cells within 100 μm of the lesion border ($n = 34$) was significantly higher than that in the cells in both the upper ($n = 34$) and the lower ($n = 40$) parts >100 μm from the lesion border (post hoc Tukey test; $^{**}P < 0.01$, 15 slices). (*D*) The number of spontaneous Ca^{2+} transients before and after bath application of BMI in each area. The frequency of Ca^{2+} transients was significantly decreased by BMI only in the area within 100 μm of the lesion border (2-tailed paired *t*-test, $^{**}P < 0.01$). Number of cells: <100 μm, 21; >100 μm; upper, 21; deeper, 18 (6 slices). (*E*) Number of spontaneous Ca^{2+} transients before and after bath application of D-AP5 and CNQX in each area. The frequency of Ca^{2+} transients was significantly decreased by D-AP5 + CNQX only in the areas >100 μm from the lesion border (paired 2-tailed *t*-test, $^{*}P < 0.05$). Number of cells: <100 μm, 13; >100 μm; upper, 13; deeper, 22 (9 slices). Scale bar: 20 μm. ACSF, artificial cerebrospinal fluid control.

superficial part was unclear and that at the boundaries of the lesioned area was apparently less cell dense (Fig. 7*A*, compare with Fig. 1*D*). At P7 ($n = 2$), although a sulcus-like formation was observed on the surface of the brain, the microgyric appearance of 3- or 4-layered cortex was obscured (Fig. 7*B*, compare with Fig. 1*E*).

Immunostaining for Cux1 (Fig. 7*C*, red) and GFP (Fig. 7*D*, green) showed a more diffuse accumulation of Cux1-positive cells in the lesioned area than that in saline-treated FFL mice (Fig. 7*C*,*E*, compare with Fig. 3*J*), and that accumulation of GABAergic cells in the superficial part and at the boundary of the lesioned area was not obvious (Fig. 7*D*,*E*, compare with Fig. 3*B–E* and Supplementary Fig. S1*B–E*). Quantitative analysis by cell counting revealed that the preferential accumulation of GFP-positive GABAergic cells in the inner rim versus the outer rim was abolished by i.p. BMI injection (Fig. 7*F*, see also Fig. 3*G*). In addition, cell density in the superficial region and the inner rim was significantly decreased by BMI treatment, while that in the outer rim was increased (Fig. 7*F*). Likewise, the preferential accumulation of Cux1-positive cortical plate cells in the outer rim versus the inner rim was abolished by i.p. BMI injection (Fig. 7*G*). We also noted the occasional invasion of Cux1-positive cortical plate cells, but not GFP-positive GABAergic cells, in the center of the lesion (Fig. 7*C–E*), which was not observed in FFL animals without BMI (compare with Fig. 3).

Discussion

The present study suggests that FFL may cause a de-differentiation of the cortical cells that accumulate in the lesion site during the formation of the microgyrus. We have demonstrated several lines of evidence for this: 1) both GABAergic and glutamatergic neurons accumulated to surround the FFL-induced necrotic center, while GABAergic neurons occupied the inner rim including the superficial region; 2) extracellular GABA was temporally increased in and around the FFL-induced necrotic center; 3) both GABAergic and glutamatergic neurons around the FFL displayed downregulated *KCC2* mRNA expression; and 4) cells located near the lesion displayed a higher frequency of spontaneous Ca^{2+} oscillation, which was activated via $GABA_A$ receptors.

Distinct Accumulation Patterns of GABAergic and Glutamatergic Neurons in FFL

Here, we distinguished between the apparent migration patterns of GABAergic and glutamatergic neurons accumulating in the area surrounding the FFL during the formation of the microgyrus. We previously described a transient cell-dense band superficial to the lesion site as a "bridge structure" that corresponded to the "dark zone" consisting of apparently migrating neurons in a rat FFL model (Dvorák and Feit 1977; Shimizu-Okabe et al. 2007). In the present study, using GAD67-GFP KI mice, we found that GABAergic neurons predominantly occupy the "bridge structure." Although a recent study showed that transient ischemia stimulates proliferation and migration of interneuron precursors in the subpial region of the neocortex (Ohira et al. 2010), newly generated neurons were not observed in the rat FFL (Rosen et al. 1996; Shimizu-Okabe et al. 2007), and no GAD67-positive (GFP-positive) proliferating (Ki67-positive) cells were observed (Supplementary Fig. S5). These results suggest that

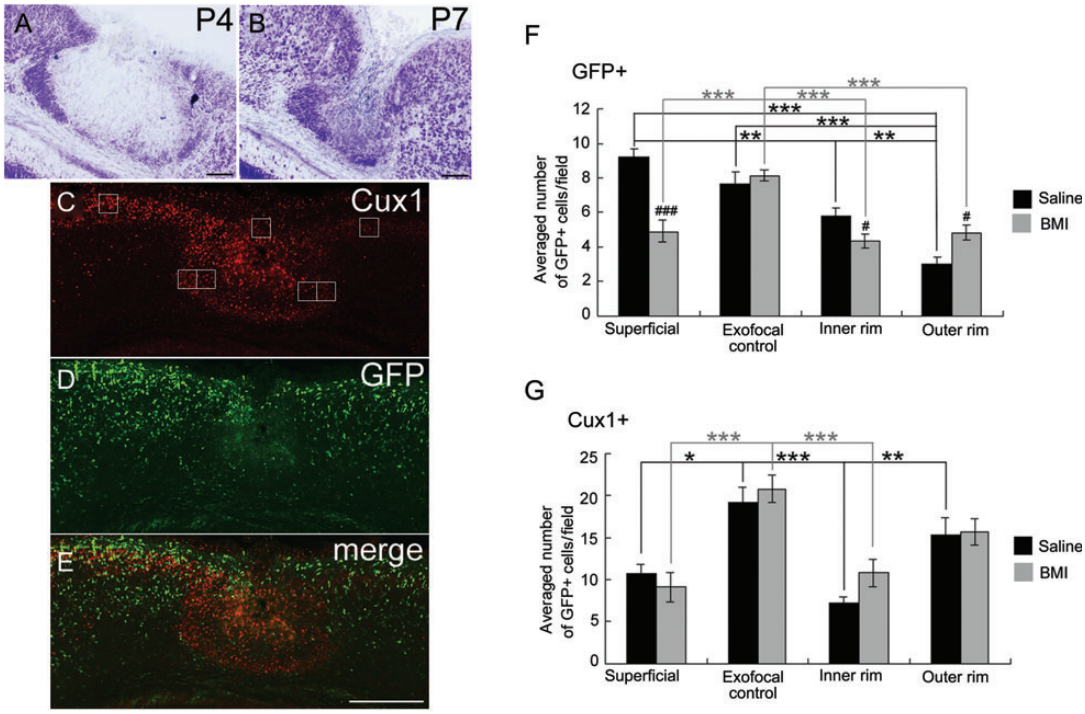

Figure 7. Distribution of late-born glutamatergic neurons and GABAergic cells in the FFL cortex at P4 after i.p. injection of bicuculline. (*A* and *B*) Thionin-stained coronal section from a P4 (*A*) and P7 (*B*) GAD67-GFP KI mouse that received FFL at P0 and i.p. injection of BMI from P2 to P4. (*C–E*) Images of a coronal section of a P4 FFL mouse that received i.p. injection of BMI, followed by immunostaining for Cux1 (red, *C*) and GFP (green, *D*). (*E*) Merged images of *C* and *D* show disturbances in the distinct distribution pattern of Cux1-positive and GFP-positive cells at the boundary of the lesioned area after in vivo application of BMI. (*F*) Effect of BMI on the distribution of GFP-positive cells in 4 different regions (superficial, exofocal control, inner rim, and outer rim). The positions of cell-count square frames (50 $\mu m \times 50\ \mu m$) are shown in *C*. Two-way ANOVA (region × drug) revealed a significant region effect ($F_{3,121} = 16.0$, $P < 0.001$), a drug effect ($F_{1,121} = 10.2$, $P < 0.01$), and a significant region × drug interaction ($F_{3,121} = 8.12$, $P < 0.001$). Note that the significant difference between the inner rim and the outer rim was abolished by the application of BMI (post hoc Tukey test, $^{**}P < 0.01$, $^{***}P < 0.001$; saline [black symbols], 5 preparations; BMI [gray symbols], 9 preparations). Significant differences in drug effects were region-specific (independent 2-tailed *t*-test, $^{\#}P < 0.05$, $^{\#\#\#}P < 0.001$). (*G*) Effect of BMI on the distribution of Cux1-positive cells in 4 different regions. Two-way ANOVA (region × drug) revealed a significant region effect ($F_{3,36} = 13.1$, $P < 0.001$). Note that the significant difference between the inner rim and the outer rim was abolished by the application of BMI (post hoc Tukey test, $^{*}P < 0.05$, $^{**}P < 0.01$, $^{***}P < 0.001$, and independent 2-tailed *t*-test, $P > 0.05$, saline [black symbols], 4 preparations; BMI [gray symbols], 7 preparations. Scale bars: *A* and *B*, 100 μm; *E*, 200 μm.

GABAergic neurons might migrate from the adjacent undamaged area to the FFL.

Consistent with a previous report (Rosen et al. 1996), late-born (E17.5) neurons, but not early-born (E14.5) neurons, became dispersed throughout layer 2 of the microgyrus. Furthermore, we characterized for the first time that the majority of late-born cells were glutamatergic pyramidal neurons, because they were negative for GFP and immunopositive for Cux1, which is specific to the pyramidal neurons of the upper layers (II–IV) of the murine cortex (Nieto et al. 2004). The area surrounding the FFL-induced necrotic center contained GABAergic neurons in the inner rim, which were surrounded by a population of late-born glutamatergic neurons (Fig. 3*C*). Before the FFL was induced, late-born glutamatergic neurons were still located in the deep layer (Supplementary Fig. S2), suggesting that these neurons may have the ability to migrate to the necrotic area and form layer 2 of the microgyrus.

Ambient GABA and Neuronal Migration

Using an enzyme-linked fluorometric assay that allowed us to image the spatial distribution of particular neurotransmitters quantitatively (Morishima et al. 2010), we found that the extracellular GABA concentration was temporally increased in the necrotic center and in the area within 100 μm of the FFL border (Fig. 4).

Medial ganglionic eminence-derived interneurons require $GABA_A$ receptor signaling to cross the corticostriatal junction, while $GABA_A$ receptor activation largely hinders the migration of interneurons in the cortical plate (Behar et al. 1996; Cuzon et al. 2006). More recently, GABA has been found to stimulate interneuron motility through depolarizing activation of $GABA_A$ receptors, and then to terminate the migration once $GABA_A$ receptor activation becomes hyperpolarizing (Bortone and Polleux 2009). This evidence supports the hypothesis that the FFL-induced temporally increased GABA further induces GABAergic neurons to migrate into and surround the GABA-rich necrotic center.

GABA-mediated responses also differently regulate radial migration of cortical neurons in a location-and-concentration-dependent manner (Behar et al. 1996, 1998, 2000; Heck et al. 2007; Denter et al. 2010). GABA stimulates the migration of projection neurons from the ventricular and subventricular zones to the intermediate zone through activation of both $GABA_A$ and $GABA_C$ receptors, while $GABA_A$ is a "stop" and $GABA_C$ is a "go" signal in the intermediate zone (Behar et al. 1998, 2000; Denter et al. 2010). On the other hand, functional inhibition of $GABA_A$ receptors induced heterotopic cell clusters in the most superficial layers, suggesting that GABA acts as a stop signal for cortical neurons once the neurons reach their final destination (Heck et al. 2007). Thus, the temporal

increase in ambient GABA in the necrotic center might initially accelerate and then stop migration of late-born cells. In other words, the high ambient GABA in the necrotic center at P4 (Fig. 4) might prevent glutamatergic neurons from entering the lesioned area (Fig. 3 and Supplementary Fig. S1, also see Fig. 7 for the negative effect induced by BMI).

Taken together, the temporally increased extracellular GABA in the lesioned site might act as a chemoattractant for the GABAergic neurons and the late-born pyramidal neurons to migrate toward the lesioned cortex in an autocrine/paracrine manner and also act to stop the latter underneath the former, contributing to the formation of the microgyrus. We might even be underestimating the effects of GABA, because heterozygous GAD67-GFP KI mice show relatively reduced ambient GABA levels in the embryo (Morishima et al. 2010), although adult levels are normal (Tamamaki et al. 2003).

The GABA concentration of about 25 μM in the area within 100 μm of the lesion border is higher than the 10 μM at >100 μm from the border; the latter is reportedly a nondesensitizing concentration for the $GABA_A$ receptors of migrating GABAergic neuronal precursors (Bolteus and Bordey 2004). However, this value is much lower than the desensitizing concentration of 100 μM (Bolteus and Bordey 2004) and, instead, is equal to the 50% effective concentration (Stewart et al. 2002)—in other words, significant $GABA_A$ receptor desensitization is unlikely. Indeed, a 10-min continuous application of 25 μM GABA to P4 control neocortical slices generated a persistent current in patch-clamped neurons (data not shown). Furthermore, the effectiveness of the $GABA_A$ receptor antagonist BMI on spontaneous Ca^{2+} transients in cells <100 μm from the FFL border indicates tonic (i.e. nondesensitizing) activation of $GABA_A$ receptors in our model.

One possible explanation for the source of ambient GABA is the GABAergic neurons that surround the necrosis. The released GABA could diffuse into the necrotic center. Alternatively, the reactive glial cells in the lesioned cortex could also provide ambient GABA, because glial cells can release GABA in a nonvesicular manner (Barakat and Bordey 2002; Park et al. 2009; Lee et al. 2010). However, this is unlikely, because GFAP-positive reactive astrocytes and Iba1-positive microglial cells in the area surrounding the necrotic center did not colocalize with GAD67 (Supplementary Fig. S6).

In contrast to the distribution of extracellular GABA, we found that the distribution of extracellular glutamate was higher in the areas far from the FFL border. The accumulation of GFAP-positive reactive astrocytes and Iba1-positive microglial cells (Supplementary Fig. S6), in the apparent absence of glutamatergic cells in the necrotic center, might explain this phenomenon. Because both astrocytes and microglia express functional glutamate transporters such as GLAST and GLT-1 (Anderson and Swanson 2000; Nakajima et al. 2001), transporter-mediated glutamate uptake may explain the reduced glutamate level in the lesioned area, resulting in the distinctive glutamate distribution in the FFL cortex.

By means of in vivo microdialysis in the adult rat hippocampus, 0.2–0.8 and 3–6 μM concentrations of GABA and glutamate, respectively, have been reported (Lerma et al. 1986; Rakovska et al. 1998). To the best of our knowledge, such information is not available for the normal developing neocortex, and estimated values vary widely according to the technique used. For example, glutamate accumulation in astrocytic culture measured with an enzyme-linked assay system using CCD imaging similar to our own was reported to be 1–100 μM (Innocenti et al. 2000). Because ambient GABA levels might be higher at more immature stages of development (Dvorzhak et al. 2010; Morishima et al. 2010), the in vivo levels of GABA and glutamate in our model could be compatible with the measured levels in this study.

CXCL12, a member of the CXC subfamily of chemokines (also known as stromal cell-derived factor 1), is expressed in the meninges and in the subventricular zone of the developing cortex and functions as a chemoattractant for the migration of GABAergic neurons expressing its receptor CXCR4 (Stumm et al. 2003, 2007; Tiveron et al. 2006; López-Bendito et al. 2008). Therefore, we considered the possibility that CXCL12/CXCR4 signaling plays a role in the accumulation of GABAergic neurons during the formation of the microgyrus at P4. However, apparent *CXCL12* and *CXCR4* mRNA signals induced by FFL were not found around the necrotic tissue at this stage (Supplementary Fig. S4). These results suggest that CXCL12/CXCR4 signaling may not be involved in the accumulation of GABAergic neurons during the development of the microgyrus.

Downregulation of KCC2 mRNA During the Formation of the Microgyrus

Under pathological conditions such as neuronal trauma or axotomy, mature neurons downregulate the expression of KCC2 and revert to a depolarizing immature-like response to GABA (Toyoda et al. 2003; for review, Payne et al. 2003). Here, a temporal downregulation of *KCC2* mRNA expression in GABAergic neurons, and in late-born glutamatergic neurons surrounding the GABA-rich necrotic center, was observed, suggesting that both GABAergic neurons and late-born glutamatergic neurons in the lesioned cortex might dedifferentiate to an immature state, with a depolarizing response to ambient GABA due to high $[Cl^-]_i$.

GABA acts as a "go" signal for immature low-*KCC2*-expressing interneurons, but acts as a "stop" signal for interneurons expressing high levels of *KCC2* once they reach the cortex (Bortone and Polleux 2009). We believe that a similar mechanism occurs during the formation of the microgyrus. A bidirectional function (motility-promoting or a stop signal) depending on the expression of *KCC2* is compatible with our results, for example, equivalent expression of *KCC2* mRNA after forming the microgyrus at P7.

Calcium Transients and Neuronal Migration

Intracellular Ca^{2+} signaling is important for controlling the migration of immature neurons (Komuro and Rakic 1992, 1996; Ben-Ari et al. 1997; Kumada and Komuro 2004; Heck et al. 2007; Bortone and Polleux 2009). The frequency of Ca^{2+} transients in immature neurons can be associated with the rate of cell movement (Komuro and Rakic 1996; Kumada and Komuro 2004). In this study, blockade of $GABA_A$ receptors reduced the frequency of spontaneous Ca^{2+} transients in cells within 100 μm, but not in cells more than 100 μm from the lesion border. This suggests that a depolarizing shift in the $GABA_A$ receptor-mediated response induced by downregulation of *KCC2* expression could lead to Ca^{2+} oscillation and facilitate the migration of both GABAergic and late-born glutamatergic neurons. Then, GABA would terminate the migration by decreasing the frequency of Ca^{2+} oscillation once the

$GABA_A$ receptor activation became hyperpolarizing (Bortone and Polleux 2009). The differential characteristics of Ca^{2+} transients between the areas <100 μm and >100 μm from the FFL border could be attributable to differences in $[Cl^-]_i$ caused by differential expression of *KCC2*, as well as a differential concentration of extracellular GABA.

In contrast to cells <100 μm from the FFL border, in the exofocal area >100 μm from the FFL border, where glutamate was abundant compared with GABA, the frequency of Ca^{2+} transients was sensitive to the glutamate receptor antagonists CNQX + D-AP5. As expected, the upper and lower exofocal cortex displayed no differences in the characteristics of their Ca^{2+} transients (Fig. 6), despite the differential *KCC2* expression (Fig. 5). Our results add a new dimension by showing that apparently migrating neurons in the area surrounding the FFL-induced necrosis can sense the high level of ambient GABA, and that this contributes to the formation of the microgyrus through Ca^{2+}-dependent mechanisms.

$GABA_A$ Receptor Activation May Underlie the Formation of the Microgyrus

Because previous reports using rats showed that FFL only during P0–1 can form a microgyrus (Dvorák et al. 1978), we conducted a control experiment, performing FFL on P2 (>48 h after birth) GAD67-GFP KI mice and investigating the morphological changes. Seven days after FFL (i.e. at P9; 2 animals), a sulcus-like formation was observed on the surface of the brain. As reported before (Dvorák et al. 1978), only defects of cortical lamination were observed, without the microgyric appearance of a 3- or 4-layered cortex (see Supplementary Fig. S7*C* and compare with Fig. 1*E*). In this negative control experiment, at 4 days after the FFL (i.e. at P6; 2 animals), the cell-dense layer was unclear both in the superficial part and at the boundaries of the lesioned area (see Supplementary Fig. S7*A* and compare with Fig. 1*D*). Interestingly, an accumulation of GABAergic cells surrounding the necrotic tissue was not detected at P6 (see Supplementary Fig. S7*B* and compare with Fig. 3*B–E* and Supplementary Fig. S1*B–E*).

Together with the results from in vivo blockade of ambient GABA action—which showed perturbation of the peculiar accumulation of GABAergic and cortical plate cells and prevention of microgyrus formation—the above findings support the following hypothesis. The temporally increased GABA causes tonic $GABA_A$ receptor activation of neurons, resulting in modulation of Ca^{2+} signaling, which differentially affects the migratory status of GABAergic ("go") and E17-born, Cux1-positive cortical plate cells ("stop") during the formation of the microgyrus.

Conclusion

Tonic $GABA_A$ receptor activation in *KCC2*-downregulated neurons by temporally increased ambient GABA regulates the distinct migration patterns of GABAergic and glutamatergic neurons via Ca^{2+} signaling during the formation of the microgyrus.

Supplementary Material

Supplementary material can be found at: http://www.cercor.oxfordjournals.org/.

Funding

This work was supported by a Grant-in-Aid for Scientific Research (grant number 19390058 to A.F.) from the Japan Society for the Promotion of Science; and by Grants-in-Aid for Scientific Research on Priority Areas: Elucidation of Neural Network Function in the Brain (grant number 20021015 to A.F.) and Molecular Interaction and Modal Shift of Cellular Sensor (grant number 21026013 to A.F.) from the Ministry of Education, Culture, Sports, Science, and Technology, Japan. Funding to pay the Open Access publication charges for this article was provided by Japan Society for the Promotion of Science.

Notes

Conflict of Interest: None declared.

References

Anderson CM, Swanson RA. 2000. Astrocyte glutamate transport: review of properties, regulation, and physiological functions. Glia. 32:1–14.

Anderson SA, Eisenstat DD, Shi L, Rubenstein JL. 1997. Interneuron migration from basal forebrain to neocortex: dependence on Dlx genes. Science. 278:474–476.

Anderson SA, Marín O, Horn C, Jennings K, Rubenstein JL. 2001. Distinct cortical migrations from the medial and lateral ganglionic eminences. Development. 128:353–363.

Barakat L, Bordey A. 2002. GAT-1 and reversible GABA transport in Bergmann glia in slices. J Neurophysiol. 88:1407–1419.

Behar TN, Li YX, Tran HT, Ma W, Dunlap V, Scott C, Barker JL. 1996. GABA stimulates chemotaxis and chemokinesis of embryonic cortical neurons via calcium-dependent mechanisms. J Neurosci. 16:1808–1818.

Behar TN, Schaffner AE, Scott CA, Greene CL, Barker JL. 2000. GABA receptor antagonists modulate postmitotic cell migration in slice cultures of embryonic rat cortex. Cereb Cortex. 10:899–909.

Behar TN, Schaffner AE, Scott CA, O'Connell C, Barker JL. 1998. Differential response of cortical plate and ventricular zone cells to GABA as a migration stimulus. J Neurosci. 18:6378–6387.

Behar TN, Smith SV, Kennedy RT, McKenzie JM, Maric I, Barker JL. 2001. GABA(B) receptors mediate motility signals for migrating embryonic cortical cells. Cereb Cortex. 11:744–753.

Ben-Ari Y. 2002. Excitatory actions of GABA during development: the nature of the nurture. Nat Rev Neurosci. 3:728–739.

Ben-Ari Y, Khazipov R, Leinekugel X, Caillard O, Gaiarsa JL. 1997. $GABA_A$, NMDA and AMPA receptors: a developmentally regulated 'ménage à trois'. Trends Neurosci. 20:523–529.

Blaesse P, Airaksinen MS, Rivera C, Kaila K. 2009. Cation-chloride cotransporters and neuronal function. Neuron. 61:820–838.

Bolteus AJ, Bordey A. 2004. GABA release and uptake regulate neuronal precursor migration in the postnatal subventricular zone. J Neurosci. 24:7623–7631.

Bortone D, Polleux F. 2009. KCC2 expression promotes the termination of cortical interneuron migration in a voltage-sensitive calcium-dependent manner. Neuron. 62:53–71.

Bulfone A, Smiga SM, Shimamura K, Peterson A, Puelles L, Rubenstein JL. 1995. T-brain-1: a homolog of Brachyury whose expression defines molecularly distinct domains within the cerebral cortex. Neuron. 15:63–78.

Chu Y, Parada I, Prince DA. 2009. Temporal and topographic alterations in expression of alpha3 isoform of Na^+, K^+-ATPase in the rat freeze-lesion model of microgyria and epileptogenesis. Neuroscience. 162:339–348.

Cuzon VC, Yeh PW, Cheng Q, Yeh HH. 2006. Ambient GABA promotes cortical entry of tangentially migrating cells derived from the medial ganglionic eminence. Cereb Cortex. 16:1377–1388.

DeFelipe J, Alonso-Nanclares L, Arellano JI. 2002. Microstructure of the neocortex: comparative aspects. J Neurocytol. 31:299–316.

Demarque M, Represa A, Becq H, Khalilov I, Ben-Ari Y, Aniksztejn L. 2002. Paracrine intercellular communication by a Ca^{2+}- and SNARE-independent release of GABA and glutamate prior to synapse formation. Neuron. 36:1051–1061.

Denter DG, Heck N, Riedemann T, White R, Kilb W, Luhmann HJ. 2010. $GABA_C$ receptors are functionally expressed in the intermediate zone and regulate radial migration in the embryonic mouse neocortex. Neuroscience. 167:124–134.

Dvorák K, Feit J. 1977. Migration of neuroblasts through partial necrosis of the cerebral cortex in newborn rats-contribution to the problems of morphological development and developmental period of cerebral microgyria. Histological and autoradiographical study. Acta Neuropathol. 38:203–212.

Dvorák K, Feit J, Juránková Z. 1978. Experimentally induced focal microgyria and status verrucosus deformis in rats–pathogenesis and interrelation. Histological and autoradiographical study. Acta Neuropathol. 44:121–129.

Dvorzhak A, Myakhar O, Unichenko P, Kirmse K, Kirischuk S. 2010. Estimation of ambient GABA levels in layer I of the mouse neonatal cortex in brain slices. J Physiol. 588:2351–2360.

Francis F, Meyer G, Fallet-Bianco C, Moreno S, Kappeler C, Socorro AC, Tuy FP, Beldjord C, Chelly J. 2006. Human disorders of cortical development: from past to present. Eur J Neurosci. 23:877–893.

Fukuda A, Muramatsu K, Okabe A, Shimano Y, Hida H, Fujimoto I, Nishino H. 1998. Changes in intracellular Ca^{2+} induced by $GABA_A$ receptor activation and reduction in Cl^- gradient in neonatal rat neocortex. J Neurophysiol. 79:439–446.

Hagemann G, Kluska MM, Redecker C, Luhmann HJ, Witte OW. 2003. Distribution of glutamate receptor subunits in experimentally induced cortical malformations. Neuroscience. 117:991–1002.

Heck N, Kilb W, Reiprich P, Kubota H, Furukawa T, Fukuda A, Luhmann HJ. 2007. GABA-A receptors regulate neocortical neuronal migration in vitro and in vivo. Cereb Cortex. 17:138–148.

Heng JI, Moonen G, Nguyen L. 2007. Neurotransmitters regulate cell migration in the telencephalon. Eur J Neurosci. 26:537–546.

Ignacio MP, Kimm EJ, Kageyama GH, Yu J, Robertson RT. 1995. Postnatal migration of neurons and formation of laminae in rat cerebral cortex. Anat Embryol (Berl). 191:89–100.

Innocenti B, Parpura V, Haydon PG. 2000. Imaging extracellular waves of glutamate during calcium signaling in cultured astrocytes. J Neurosci. 20:1800–1808.

Jacobs KM, Gutnick MJ, Prince DA. 1996. Hyperexcitability in a model of cortical maldevelopment. Cereb Cortex. 6:514–523.

Jacobs KM, Prince DA. 2005. Excitatory and inhibitory postsynaptic currents in a rat model of epileptogenic microgyria. J Neurophysiol. 93:687–696.

Jimbu T, Inoue N, Ohtani S, Hozumi N, Yoshida S. 2009. Detection of synaptic glutamate release in cerebellar cortex using covalent immobilized enzyme assay and UV-LED excitation system. Presented at the 32nd Annual Meeting of the Japan Neuroscience Society, Nagoya, Japan, Sep 16–18, 2009. Program No. P2-a26.

Kharazia VN, Jacobs KM, Prince DA. 2003. Light microscopic study of GluR1 and calbindin expression in interneurons of neocortical microgyral malformations. Neuroscience. 120:207–218.

Komuro H, Kumada T. 2005. Ca^{2+} transients control CNS neuronal migration. Cell Calcium. 37:387–393.

Komuro H, Rakic P. 1996. Intracellular Ca^{2+} fluctuations modulate the rate of neuronal migration. Neuron. 17:275–285.

Komuro H, Rakic P. 1992. Selective role of N-type calcium channels in neuronal migration. Science. 257:806–809.

Kumada T, Komuro H. 2004. Completion of neuronal migration regulated by loss of Ca^{2+} transients. Proc Natl Acad Sci USA. 101:8479–8484.

Lavdas AA, Grigoriou M, Pachnis V, Parnavelas JG. 1999. The medial ganglionic eminence gives rise to a population of early neurons in the developing cerebral cortex. J Neurosci. 19:7881–7888.

Lee S, Yoon BE, Berglund K, Oh SJ, Park H, Shin HS, Augustine GJ, Lee CJ. 2010. Channel-mediated tonic GABA release from glia. Science. 330:790–796.

Lerma J, Herranz AS, Herreras O, Abraira V, Martin del Rio R. 1986. In vivo determination of extracellular concentration of amino acids in the rat hippocampus: a method based on brain dialysis and computerized analysis. Brain Res. 384:145–155.

López-Bendito G, Luján R, Shigemoto R, Ganter P, Paulsen O, Molnár Z. 2003. Blockade of $GABA_B$ receptors alters the tangential migration of cortical neurons. Cereb Cortex. 13:932–942.

López-Bendito G, Sánchez-Alcañiz JA, Pla R, Borrell V, Picó E, Valdeolmillos M, Marín O. 2008. Chemokine signaling controls intracortical migration and final distribution of GABAergic interneurons. J Neurosci. 28:1613–1624.

Luhmann HJ, Karpuk N, Qü M, Zilles K. 1998. Characterization of neuronal migration disorders in neocortical structures. II. Intracellular in vitro recordings. J Neurophysiol. 80:92–102.

Luhmann HJ, Raabe K. 1996. Characterization of neuronal migration disorders in neocortical structures: I. Expression of epileptiform activity in an animal model. Epilepsy Res. 26:67–74.

Luján R, Shigemoto R, López-Bendito G. 2005. Glutamate and GABA receptor signalling in the developing brain. Neuroscience. 130:567–580.

Manent JB, Demarque M, Jorquera I, Pellegrino C, Ben-Ari Y, Aniksztejn L, Represa A. 2005. A noncanonical release of GABA and glutamate modulates neuronal migration. J Neurosci. 25:4755–4765.

Manent JB, Represa A. 2007. Neurotransmitters and brain maturation: early paracrine actions of GABA and glutamate modulate neuronal migration. Neuroscientist. 13:268–279.

Marín O, Rubenstein JL. 2001. A long, remarkable journey: tangential migration in the telencephalon. Nat Rev Neurosci. 2:780–790.

Miyoshi G, Fishell G. 2011. GABAergic interneuron lineages selectively sort into specific cortical layers during early postnatal development. Cereb Cortex. 21:845–852.

Morishima T, Uematsu M, Furukawa T, Yanagawa Y, Fukuda A, Yoshida S. 2010. GABA imaging in brain slices using immobilized enzyme-linked photoanalysis. Neurosci Res. 67:347–353.

Nadarajah B, Parnavelas JG. 2002. Modes of neuronal migration in the developing cerebral cortex. Nat Rev Neurosci. 3:423–432.

Nakajima K, Tohyama Y, Kohsaka S, Kurihara T. 2001. Ability of rat microglia to uptake extracellular glutamate. Neurosci Lett. 307:171–174.

Nakamura KC, Kameda H, Koshimizu Y, Yanagawa Y, Kaneko T. 2008. Production and histological application of affinity-purified antibodies to heat-denatured green fluorescent protein. J Histochem Cytochem. 56:647–657.

Nieto M, Monuki ES, Tang H, Imitola J, Haubst N, Khoury SJ, Cunningham J, Gotz M, Walsh CA. 2004. Expression of Cux-1 and Cux-2 in the subventricular zone and upper layers II-IV of the cerebral cortex. J Comp Neurol. 479:168–180.

Ohira K, Furuta T, Hioki H, Nakamura KC, Kuramoto E, Tanaka Y, Funatsu N, Shimizu K, Oishi T, Hayashi M et al. 2010. Ischemia-induced neurogenesis of neocortical layer 1 progenitor cells. Nat Neurosci. 13:173–179.

Owens DF, Kriegstein AR. 2002. Is there more to GABA than synaptic inhibition? Nat Rev Neurosci. 3:715–727.

Park H, Oh SJ, Han KS, Woo DH, Park H, Mannaioni G, Traynelis SF, Lee CJ. 2009. Bestrophin-1 encodes for the Ca^{2+}-activated anion channel in hippocampal astrocytes. J Neurosci. 29:13063–13073.

Patrick SL, Connors BW, Landisman CE. 2006. Developmental changes in somatostatin-positive interneurons in a freeze-lesion model of epilepsy. Epilepsy Res. 70:161–171.

Payne JA, Rivera C, Voipio J, Kaila K. 2003. Cation-chloride co-transporters in neuronal communication, development and trauma. Trends Neurosci. 26:199–206.

Rakic P. 1972. Mode of cell migration to the superficial layers of fetal monkey neocortex. J Comp Neurol. 145:61–83.

Rakic P. 1988. Specification of cerebral cortical areas. Science. 241:170–176.

Rakovska A, Giovannini MG, Della Corte L, Kalfin R, Bianchi L, Pepeu G. 1998. Neurotensin modulation of acetylcholine and GABA release from the rat hippocampus: an in vivo microdialysis study. Neurochem Int. 33:335–340.

Ramos RL, Bai J, LoTurco JJ. 2006. Heterotopia formation in rat but not mouse neocortex after RNA interference knockdown of DCX. Cereb Cortex. 16:1323–1331.
Redecker C, Luhmann HJ, Hagemann G, Fritschy JM, Witte OW. 2000. Differential downregulation of $GABA_A$ receptor subunits in widespread brain regions in the freeze-lesion model of focal cortical malformations. J Neurosci. 20:5045–5053.
Represa A, Ben-Ari Y. 2005. Trophic actions of GABA on neuronal development. Trends Neurosci. 28:278–283.
Rivera C, Voipio J, Payne JA, Ruusuvuori E, Lahtinen H, Lamsa K, Pirvola U, Saarma M, Kaila K. 1999. The K^+/Cl^- co-transporter KCC2 renders GABA hyperpolarizing during neuronal maturation. Nature. 397:251–255.
Rosen GD, Jacobs KM, Prince DA. 1998. Effects of neonatal freeze-lesions on expression of parvalbumin in rat neocortex. Cereb Cortex. 8:753–761.
Rosen GD, Press DM, Sherman GF, Galaburda AM. 1992. The development of induced cerebrocortical microgyria in the rat. J Neuropath Exp Neurol. 51:601–611.
Rosen GD, Sherman GF, Galaburda AM. 1996. Birthdates of neurons in induced microgyria. Brain Res. 727:71–78.
Shimizu-Okabe C, Okabe A, Kilb W, Sato K, Luhmann HJ, Fukuda A. 2007. Changes in the expression of cation-Cl^- cotransporters, NKCC1 and KCC2, during cortical malformation induced by neonatal freeze-lesion. Neurosci Res. 59:288–295.
Spitzer NC. 2008. Calcium: first messenger. Nat Neurosci. 11:243–244.
Stewart RR, Hoge GJ, Zigova T, Luskin MB. 2002. Neural progenitor cells of the neonatal rat anterior subventricular zone express functional $GABA_A$ receptors. J Neurobiol. 50:305–322.
Stumm R, Kolodziej A, Schulz S, Kohtz JD, Hollt V. 2007. Patterns of SDF-1alpha and SDF-1gamma mRNAs, migration pathways, and phenotypes of CXCR4-expressing neurons in the developing rat telencephalon. J Comp Neurol. 502:382–399.
Stumm KR, Zhou C, Ara T, Lazarini F, Dubois-Dalcq M, Nagasawa T, Höllt V, Schulz S. 2003. CXCR4 regulates interneuron migration in the developing neocortex. J Neurosci. 23:5123–5130.
Takahashi T, Nowakowski RS, Caviness VS Jr. 1995. The cell cycle of the pseudostratified ventricular epithelium of the embryonic murine cerebral wall. J Neurosci. 15:6046–6057.
Tamamaki N, Fujimori KE, Takauji R. 1997. Origin and route of tangentially migrating neurons in the developing neocortical intermediate zone. J Neurosci. 17:8313–8323.
Tamamaki N, Yanagawa T, Tomioka R, Miyazaki J, Obata K, Kaneko T. 2003. Green fluorescent protein expression and colocalization with calretinin, parvalbumin, and somatostatin in the GAD67-GFP knock-in mouse. J Comp Neurol. 467:60–79.
Tanaka DH, Maekawa K, Yanagawa Y, Obata K, Murakami F. 2006. Multidirectional and multizonal migration of GABAergic interneurons in the developing cerebral cortex. Development. 133:2167–2176.
Tiveron MC, Rossel M, Moepps B, Zhang YL, Seidenfaden R, Favor J, Konig N, Cremer H. 2006. Molecular interaction between projection neuron precursors and invading interneurons via stromal-derived factor 1 (CXCL12)/CXCR4 signaling in the cortical subventricular zone/intermediate zone. J Neurosci. 26: 13273–13278.
Toyoda H, Ohno K, Yamada J, Ikeda M, Okabe A, Sato K, Hashimoto K, Fukuda A. 2003. Induction of NMDA and $GABA_A$ receptor-mediated Ca^{2+} oscillations with KCC2 mRNA downregulation in injured facial motoneurons. J Neurophysiol. 89:1353–1362.
Walsh CA. 1999. Genetic malformations of the human cerebral cortex. Neuron. 23:19–29.
Wang DD, Kriegstein AR. 2009. Defining the role of GABA in cortical development. J Physiol. 587:1873–1879.
Yamada J, Okabe A, Toyoda H, Kilb W, Luhmann HJ, Fukuda A. 2004. Cl^- uptake promoting depolarizing GABA actions in immature rat neocortical neurones is mediated by NKCC1. J Physiol. 557:829–841.
Zilles K, Qü M, Schleicher A, Luhmann HJ. 1998. Characterization of neuronal migration disorders in neocortical structures: quantitative receptor autoradiography of ionotropic glutamate, $GABA_A$ and $GABA_B$ receptors. Eur J Neurosci. 10:3095–3106.